Cell Reports

Report

High-Throughput Drug Screening Identifies Pazopanib and Clofilium Tosylate as Promising Treatments for Malignant Rhabdoid Tumors

Graphical Abstract

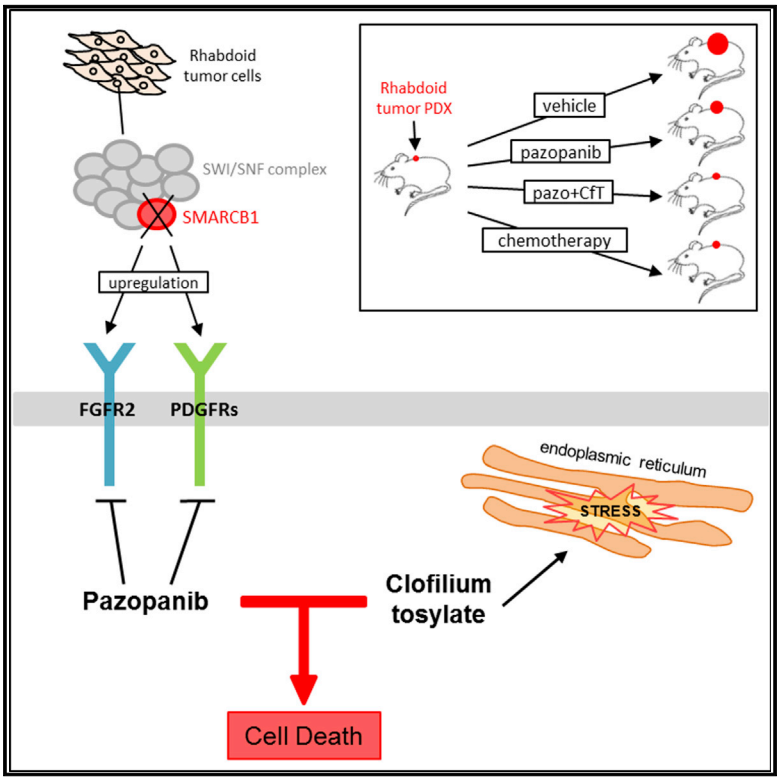

Highlights

- High-throughput screening identifies pazopanib and clofilium tosylate for rhabdoid tumors
- PDGFRα/β and FGFR2 are identified as targets of pazopanib
- Pazopanib combined with clofilium tosylate induces apoptosis of RT cells
- Reduction of PDX tumor growth by pazopanib is enhanced by the combination with CfT

Authors

Céline Chauvin, Amaury Leruste, Arnault Tauziede-Espariat, ..., Olivier Delattre, Elaine Del Nery, Franck Bourdeaut

Correspondence

franck.bourdeaut@curie.fr

In Brief

Rhabdoid tumors (RTs) are aggressive pediatric tumors characterized by SMARCB1 inactivation. Chauvin et al. identify two SMARCB1-dependent targeted therapies for RT: pazopanib, which inhibits PDGFR and FGFR2, and the potassium channel inhibitor clofilium tosylate, which induces endoplasmic reticulum stress. Combining both drugs induces cell apoptosis and reduces PDX tumor growth.

Data and Software Availability

GSE98277
GSE102467

Chauvin et al., 2017, Cell Reports *21*, 1737–1745
November 14, 2017
https://doi.org/10.1016/j.celrep.2017.10.076

CellPress

Cell Reports
Report

High-Throughput Drug Screening Identifies Pazopanib and Clofilium Tosylate as Promising Treatments for Malignant Rhabdoid Tumors

Céline Chauvin,[1,2] Amaury Leruste,[1,2] Arnault Tauziede-Espariat,[3] Mamy Andrianteranagna,[1,2] Didier Surdez,[2] Aurianne Lescure,[4] Zhi-Yan Han,[1,2] Elodie Anthony,[4] Wilfrid Richer,[1,2] Sylvain Baulande,[5] Mylène Bohec,[5] Sakina Zaidi,[2] Marie-Ming Aynaud,[2] Laetitia Maillot,[6] Julien Masliah-Planchon,[6] Stefano Cairo,[7,8] Sergio Roman-Roman,[4] Olivier Delattre,[1,2,6] Elaine Del Nery,[4] and Franck Bourdeaut[1,2,9,10,*]

[1]Paris-Sciences-Lettres Research University, Institut Curie Research Center, SiRIC, Laboratory of Translational Research in Pediatric Oncology, Paris 75005, France
[2]Paris-Sciences-Lettres Research University, Institut Curie Research Center, INSERM U830, Laboratory of Biology and Genetics of Cancers, Paris 75005, France
[3]Sainte-Anne Hospital, Department of Neuropathology, Paris 75005, France
[4]Paris-Sciences-Lettres Research University, Institut Curie, Department of Translational Research, the Biophenics High-Content Screening Laboratory, Cell and Tissue Imaging Facility (PICT-IBiSA), Paris 75005, France
[5]Paris-Sciences-Lettres Research University, Institut Curie, Next Generation Sequencing Platform, Paris 75005, France
[6]Paris-Sciences-Lettres Research University, Institut Curie, Laboratory of Somatic Genetics, Paris 75005, France
[7]LTTA Center, Department of Morphology, Surgery and Experimental Medicine, University of Ferrara, Ferrara 44121, Italy
[8]XenTech, Evry 91000, France
[9]Paris-Sciences-Lettres Research University, Institut Curie Hospital, Department of Pediatric Oncology- Adolescents and Young Adults, Paris 75005, France
[10]Lead Contact
*Correspondence: franck.bourdeaut@curie.fr
https://doi.org/10.1016/j.celrep.2017.10.076

SUMMARY

Rhabdoid tumors (RTs) are aggressive tumors of early childhood characterized by SMARCB1 inactivation. Their poor prognosis highlights an urgent need to develop new therapies. Here, we performed a high-throughput screening of approved drugs and identified broad inhibitors of tyrosine kinase receptors (RTKs), including pazopanib, and the potassium channel inhibitor clofilium tosylate (CfT), as SMARCB1-dependent candidates. Pazopanib targets were identified as PDGFRα/β and FGFR2, which were the most highly expressed RTKs in a set of primary tumors. Combined genetic inhibition of both these RTKs only partially recapitulated the effect of pazopanib, emphasizing the requirement for broad inhibition. CfT perturbed protein metabolism and endoplasmic reticulum stress and, in combination with pazopanib, induced apoptosis of RT cells *in vitro*. *In vivo*, reduction of tumor growth by pazopanib was enhanced in combination with CfT, matching the efficiency of conventional chemotherapy. These results strongly support testing pazopanib/CfT combination therapy in future clinical trials for RTs.

INTRODUCTION

Rhabdoid tumors (RTs) are rare aggressive cancers of infancy and early childhood that arise in the brain, kidney, liver, and miscellaneous soft-tissues and are characterized by biallelic inactivation of the *SMARCB1* gene (Versteege et al., 1998). Although combined in intensive protocols, conventional chemotherapy and radiotherapy allow only moderate tumor control, equating to 30% 3-year event-free survival (Brennan et al., 2016), with concerning toxicity. Seeking new therapeutic combinations is therefore of great urgency. Recent efforts have focused on restoring biological functions lost by *SMARCB1* deficiency, such as G1-to-S transition (Smith et al., 2008), or epigenetic factors, such as histone deacetylase (Kerl et al., 2013; Muscat et al., 2016) and the polycomb repressor complex 2 (PRC2) (Knutson et al., 2013). Others have studied the effects of drugs of interest, such as tyrosine kinase inhibitors (TKi's) on various cell lines and thereby identified some efficacy of one compound on RT cell lines (Wong et al., 2016). Some of these promising results are now being translated into the clinic (Geoerger et al., 2017). Finally, other strategies rely on new administration modalities of previously approved drugs ("drug repositioning"); metronomic treatments using fenofibrate, celecoxib, and thalidomide, for instance, have shown considerable promise in RT treatment (Robison et al., 2014).

Drug repurposing is a valuable route to rapid drug development (Bertolini et al., 2015) because of the known toxicology and pharmacology lower regulatory barriers and cost. Finding relevant new therapies for patients by drug repositioning is particularly relevant in pediatrics, given the lower number of early-phase trials compared with adult oncology. RTs can therefore be good candidates for such experimental investigations. One way to identify promising anti-cancer therapies is to perform large-scale pharmaceutical screenings, which blindly assess both anti-cancer and non-cancer drug activities (Raynal et al.,

2017). Large-scale drug screening also paves the way for potential successful combinations with several identified "hits." Here, we report results from screening a 1,200 approved-drug library to selectively inhibit SMARCB1-deficient cells. Thereby, we identified one antiarrhythmic agent (clofilium tosylate [CfT]) and broad TKi's such as vatalanib, ponatinib, and pazopanib, in keeping with recent reports. We found that several tyrosine kinase receptors (RTKs) must be targeted together to recapitulate the *in vitro* toxicity of broad TKi's. Finally, we show that the combination of the two main hits from our screening, CfT and pazopanib, delays tumor growth *in vivo* with an efficacy comparable to that of conventional chemotherapies currently used in the clinic.

RESULTS

High-Throughput Screening of US Food and Drug Administration-Approved Drugs Identified Vatalanib and CfT

To identify new therapeutic candidates, we screened the Prestwick Chemical Library, containing 1,200 approved molecules, on the G401 cell line and the I2A inducible cell line in the presence or absence (I2A + SMARCB1, hereafter named I2A+) of doxycycline in order to identify drugs specific for SMARCB1-deficient cells. The percentage of cytotoxic drugs (robust *Z* [RZ] score <-2) in G401, I2A and I2A+ cells was 14%, 21%, and 17%, respectively (Figure 1A; Table S1). Following the selection criteria detailed in Figure S1B, we finally selected (1) compounds showing a RZ score <-5 in at least one RT cell line (I2A or G401 cells) and showing no activity in I2A+ cells (RZ score >-2), which comprised 5 drugs (5-fluorouracil, luteolin, rimexolone, amethopterin [R,S], and methotrexate); and (2) compounds with some weak activity in I2A+ cells ($-5 <$ RZ score <-2) and showing a strong effect in at least one RT cell line (RZ score <-10) and a differential between I2A+ and I2A exceeding 2, leading to the selection of an additional 5 compounds (CfT, podophyllotoxin, ciclopirox ethanolamine, thioguanosine, and vatalanib). Altogether, we identified 10 compounds that inhibited I2A and/or G401 viability significantly more effectively than I2A+.

Confirmation of the Candidate Drugs

To demonstrate that clinically relevant hits can be identified with our screening setup, we performed dose-response curves for the 10 candidate drugs. Six compounds showed a half maximal inhibitory concentration (IC_{50}) <10 μM in both SMARCB1-deficient cell lines (Table 1; Figure S1C), belonging to distinct therapeutic groups: four conventional anti-mitotic agents (amethopterin [R,S], methotrexate, podophyllotoxin, and thioguanosine); one antiarrhythmic agent (CfT), and one broad TKi (vatalanib). To focus on innovative therapies, anti-mitotics were not considered further. Vatalanib and CfT, the two remaining compounds, were tested on a larger panel of 7 SMARCB1-negative RT cell lines and compared to 5 SMARCB1-positive cell lines (I2A+, slowly cycling, in 2 conditions and 4 rapidly cycling non-RT cells). *In vitro* treatment with vatalanib or CfT inhibited SMARCB1-negative cell growth (IC_{50} median = 5.1 μM or 4.2 μM, respectively), whereas SMARCB1-positive cell lines were significantly less affected (IC_{50} median = 10.8 μM or 15.5 μM, respectively) (Figure 1B).

Human RT Cell Lines Are Specifically Sensitive to Pazopanib

Vatalanib was the only TKi identified in the screen, but confirmation assessments revealed a high IC_{50}. Hence, we investigated whether other TKi's were more potent (i.e., IC_{50} <1 μM). Among the 9 other US Food and Drug Administration (FDA)-approved TKi's tested, ponatinib, axitinib, nintedanib, pazopanib, and dasatinib showed an IC_{50} median ≤ 1 μM (0.13, 0.3, 0.6, 0.8, and 1 μM, respectively), whereas crenolanib, CP-673451, telatinib, and amuvatinib were less efficient (IC_{50} median = 2.1, 3.1, 3.9, and 20.6 μM, respectively) (Figure 1C). The highest differential between SMARCB1-negative and SMARCB1-positive cell lines was found with pazopanib ($p = 0.001$), suggesting that the SMARCB1-dependent effect of TKi is maximal for this drug.

Phosphoproteomic Screen Identifies PDGFRα/β and FGFR2 as Targets of Pazopanib in RTs

To identify RTKs targeted by pazopanib, we assessed the phosphorylation of 49 RTKs upon treatment of the I2A, DEV, G401, and KD cell lines using the Proteome Profiler human phospho-RTK array. Among all RTKs inhibited by pazopanib (listed in Figure S2), only two were impacted in the four cell lines: (1) platelet-derived growth factor receptors (PDGFRs; PDGFRα in I2A and DEV and PDGFRβ in G401 and KD), for which we detected the strongest signal in DMSO-treated cells, and (2) fibroblast growth factor receptor 2 (FGFR2), albeit with lower intensity than PDGFRs (Figures 2A and S2).

To validate PDGFR and FGFR2 activity and sensitivity to pazopanib, we submitted I2A, DEV, G401, and KD cells to basic fibroblast growth factor (bFGF) or platelet-derived growth factor (PDGF) stimulation, either alone or upon pazopanib treatment. PDGF activation of PDGFRα in I2A and DEV cells and PDGFRβ in G401 and KD cells (Figure 2B) was efficiently inhibited by pazopanib in all 4 cell lines. The downstream effectors ERK1/2 and AKT were also activated by PDGF and inhibited by pazopanib, with a lesser effect observed in KD cells. Similar results were observed for bFGF signaling, which activates ERK1/2 (Figure 2B).

PDGFRs and FGFR2 Are Expressed in Primary RTs and Dependent upon *SMARCB1* Loss

We next analyzed whether PDGFRs and FGFR are relevant targets for further studies in humans. RTKs for which phosphorylation was inhibited by pazopanib in more than one cell line (Figure S2) were ordered according to their expression level in primary tumors; PDGFRα, FGFR2, and PDGFRβ were the highest expressed RTKs (Figure 2C).

We then analyzed how expression of RTK and downstream effectors were affected by *SMARCB1* using the I2A inducible cells. None of the RTK varied in expression level upon *SMARCB1* re-expression, except *PDGFRα* and *FGFR2* (Figure 2D); we also noticed a significant variation in downstream inhibitors, such as *DUSP1*, *DUSP9*, and *SPRY2* (Figure S3A). Thus, *PDGFR* and *FGFR2*, the two consensus signaling targets of pazopanib in our cell lines, are the most highly expressed RTKs in primary

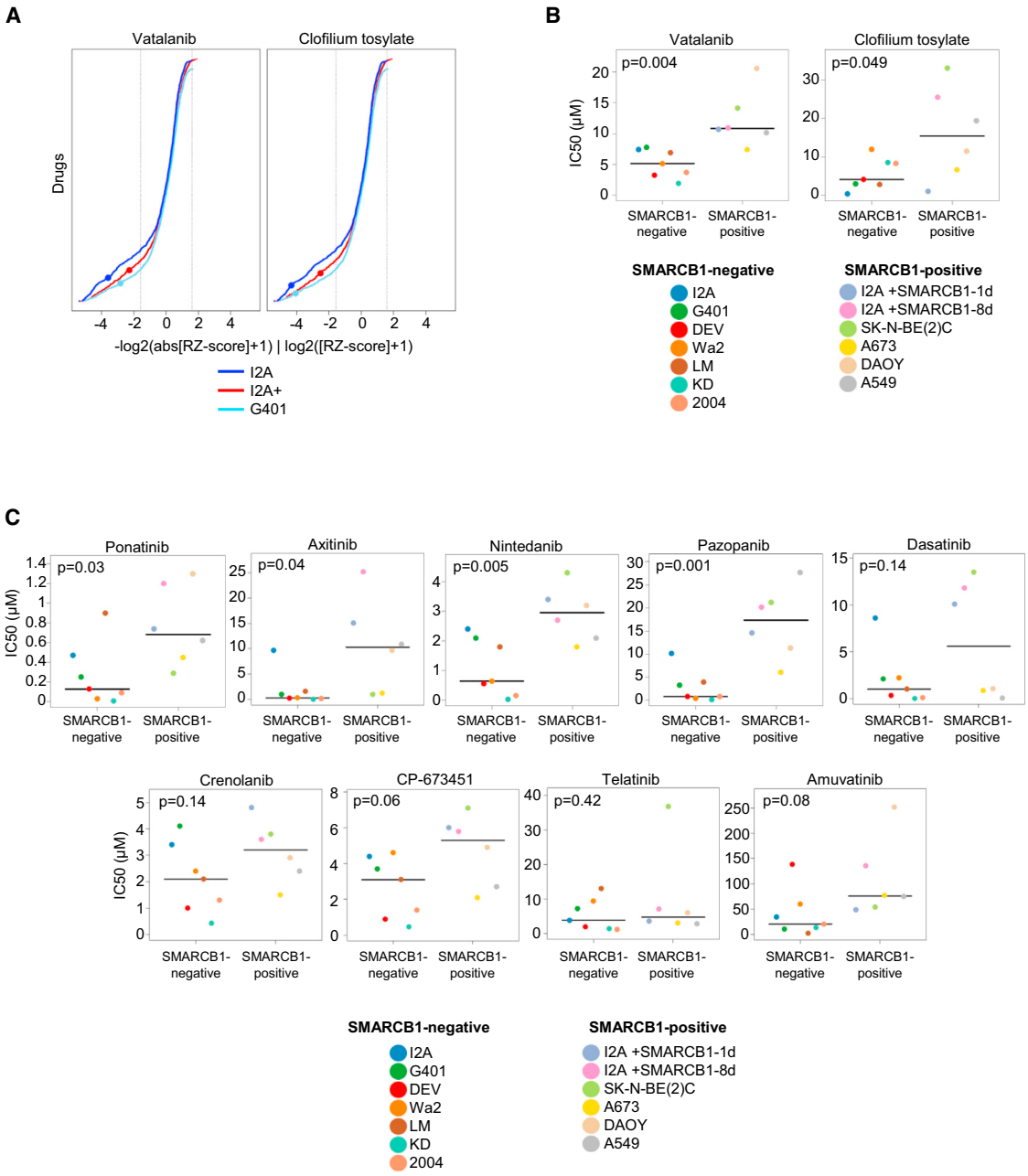

Figure 1. High-Throughput Drug Screening Identifies Vatalanib and CfT

(A) Distribution of RZ scores of 1,200 molecules from the Prestwick Chemical Library in I2A, I2A+, and G401 cell lines. x axis: if the RZ score was negative or positive, the formula $-\log2(\text{abs}[\text{RZ score}] + 1)$ or $\log2([\text{RZ score}] + 1)$ was used, respectively. Line color indicates the cell line. Dots correspond to the drug indicated above the panel. RZ score data are provided in Table S1.

(B and C) IC_{50} values of vatalanib and clofilium tosylate (B) or expanded series of TKi (C), normalized to DMSO control, in 7 SMARCB1-negative and 6 SMARCB1-positive cell lines (I2A at day 1 or day 8 after DOX withdrawal). Dots represent the mean of 2–3 independent experiments; horizontal lines represent the median. p values were obtained by two-tailed unpaired Student's t test.

tumors, and their expression, together with various signaling effectors, is regulated by *SMARCB1*. Furthermore, analysis of publicly available data on human samples (Johann et al., 2016) revealed a striking low methylation of *PDGFRα* and *FGFR2* promoters (Figures S3B–S3D); in contrast, chromatin immunoprecipitation sequencing (ChIP-seq) data in the G401 cell line (Wang et al., 2017) showed no histone modification in enhancer regions upon *SMARCB1* re-expression (Figures S3E and S3F). Together, these findings suggest that *SMARCB1* regulates RTK expression via promoter methylation.

Table 1. RZ Scores (Median of Replicates) and IC_{50} Values in I2A, G401, and I2A+ Cell Lines for the 10 Selected Hits

		RZ Scores (Median of Replicates)			IC_{50} (μM)		
Perturbator	Therapeutic Group	I2A	G401	I2A+	I2A	G401	I2A+
5-Fluorouracil	chemotherapy	−2.07	−15.57	−1.57	78.9	0.8	37.7
Luteolin	expectorant	−8.54	−5.34	−1.11	25.3	11.7	27.3
Rimexolone	glucocorticoid steroid	−2.26	−8.84	−1.72	47.0	8.0	32.0
Amethopterin (R,S)	chemotherapy	−3.35	−7.32	−1.34	0.07	0.3	7.6
Methotrexate	chemotherapy	−3.38	−7.29	−1.76	0.08	0.3	0.4
CfT	antiarrhythmic	−19.30	−15.93	−4.77	0.4	3.0	1.1
Podophyllotoxin	chemotherapy	−7.45	−17.73	−4.78	0.02	0.01	0.1
Ciclopirox ethanolamine	antifungal	−9.63	−11.94	−3.61	50.9	5.7	41.0
Thioguanosine	chemotherapy	−8.63	−11.55	−4.74	5.3	2.5	7.4
Vatalanib	RTK inhibitor	−11.24	−6.24	−3.88	7.4	7.8	10.7

Dual Depletion of PDGFR and FGFR2 Partly Recapitulates the Effect of Pazopanib on RT Cell Lines

To confirm the sensitivity of SMARCB1-deficient cells to FGFR2 and/or PDGFRα/β inhibition, we investigated whether depletion of PDGFRs or FGFR2 could recapitulate the effect of pazopanib. To this aim, I2A, DEV, G401, and KD cells were transfected with small interfering RNA (siRNA) against FGFR2 and/or PDGFRα (I2A and DEV) and FGFR2 and/or PDGFRβ (G401 and KD). Despite a strong knockdown effect of the siRNAs (Figure 2E), PDGFR and FGFR2 depletion did not affect RT cell viability (Figure 2F) or apoptosis (Figure 2G). In contrast, co-depleting PDGFRα and FGFR2 in I2A and DEV cells and PDGFRβ and FGFR2 in G401 and KD cells significantly decreased cell viability in all four RT cell lines, but not in control I2A+ cells (Figure 2F). In I2A, G401, and KD cells, a significant increase in apoptosis was also induced by dual depletion compared to control cells (Figure 2G), and this was related to decreased AKT phosphorylation (data not shown). Thus, PDGFR or FGFR2 depletion alone is insufficient to phenocopy the effect of pazopanib, which was better recapitulated by dual RTK inactivation.

Combinatory Treatment of Pazopanib and CfT Induces Apoptosis in RTs

To circumvent potential resistance to single therapies, we investigated whether pazopanib and CfT could potentiate each other when used in combination. We thus exposed 4 SMARCB1-deficient RT cell lines and 4 SMARCB1-positive cell lines to pazopanib at IC_{50} concentrations combined with CfT at intermediate concentration (2.5 μM) and assessed toxicity by two methods, Annexin V (Figure 3A) and resazurin (data not shown). Pazopanib treatment significantly induced apoptosis when compared to DMSO-treated cells in all RT cell lines tested except G401, whereas no apoptosis was observed in CfT-treated cells. When pazopanib was combined with CfT, a significant increase in apoptosis was detected in all 4 RT cell lines, whereas 3 out of 4 SMARCB1-positive cell lines were significantly less affected. Thus, our results suggest some specific vulnerability of RT cell lines to the pro-apoptotic activity of pazopanib combined with CfT. To understand the biological effects of CfT, we submitted I2A, DEV, G401, and KD cells to bFGF or PDGF stimulation, alone or upon CfT treatment. CfT treatment affected neither protein levels of PDGFRα/β and FGFR2 nor their phosphorylation and ERK or AKT activation. However, RNA sequencing (RNA-seq) performed on DEV and G401 cells upon CfT treatment revealed striking changes in protein metabolism and endoplasmic reticulum stress (Figure S4), suggesting that TKi's and CfT induce apoptosis by two complementary mechanisms.

Pazopanib Alone or In Combination with CfT Reduces RT Growth *In Vivo*

To assess the therapeutic potential of pazopanib and CfT on RT *in vivo*, we used two RT patient-derived xenografts (PDXs), RT-001-HAM (exons 1–4, homozygous deletion) and IC-pPDX-6 (exons 1–9, homozygous deletion). In both PDXs, pazopanib treatment significantly reduced RT growth compared to vehicle-treated mice. Furthermore, association with CfT demonstrated a significant potentiation of pazopanib's antitumor effect. The combination showed a similar or even a stronger effect than standard conventional chemotherapy (etoposide and carboplatin) on the two PDXs (Figures 3B–3E). Our candidate drugs alone and in combination significantly decreased Ki67 staining (Figures 3F and 3G). Altogether, these results demonstrate the therapeutic potential of pazopanib and, further, the benefit of combining pazopanib with CfT for treating RTs.

DISCUSSION

Although no mutation or amplification in any RTK gene is found in RTs, there is emerging evidence that TKi's may be important for the clinical management of this aggressive malignancy (Huang, 2017). The first evidence showed that targeting IGF-1R induced apoptosis in BT12 and BT16 AT/RT cell lines (D'cunja et al., 2007). In addition, the EGFR-HER2 TKi lapatinib inhibited the growth of BT16 AT/RT xenografts (Singh et al., 2013; Wöhrle et al. 2013) also highlighted the potential efficacy of NVP-BGJ398, a FGFR inhibitor, on A204, G401, and G402 extra-cranial RT cell lines and related this efficacy to the dependence of FGFR on SMARCB1. Results from a wide TKi library screening recently highlighted the specific sensitivity of A204 and G402 extra-cranial RT cell lines to TKi, among several other sarcomas (Wong et al. 2016). In keeping with our findings, they identified pazopanib as an active agent in RTs, although no preclinical

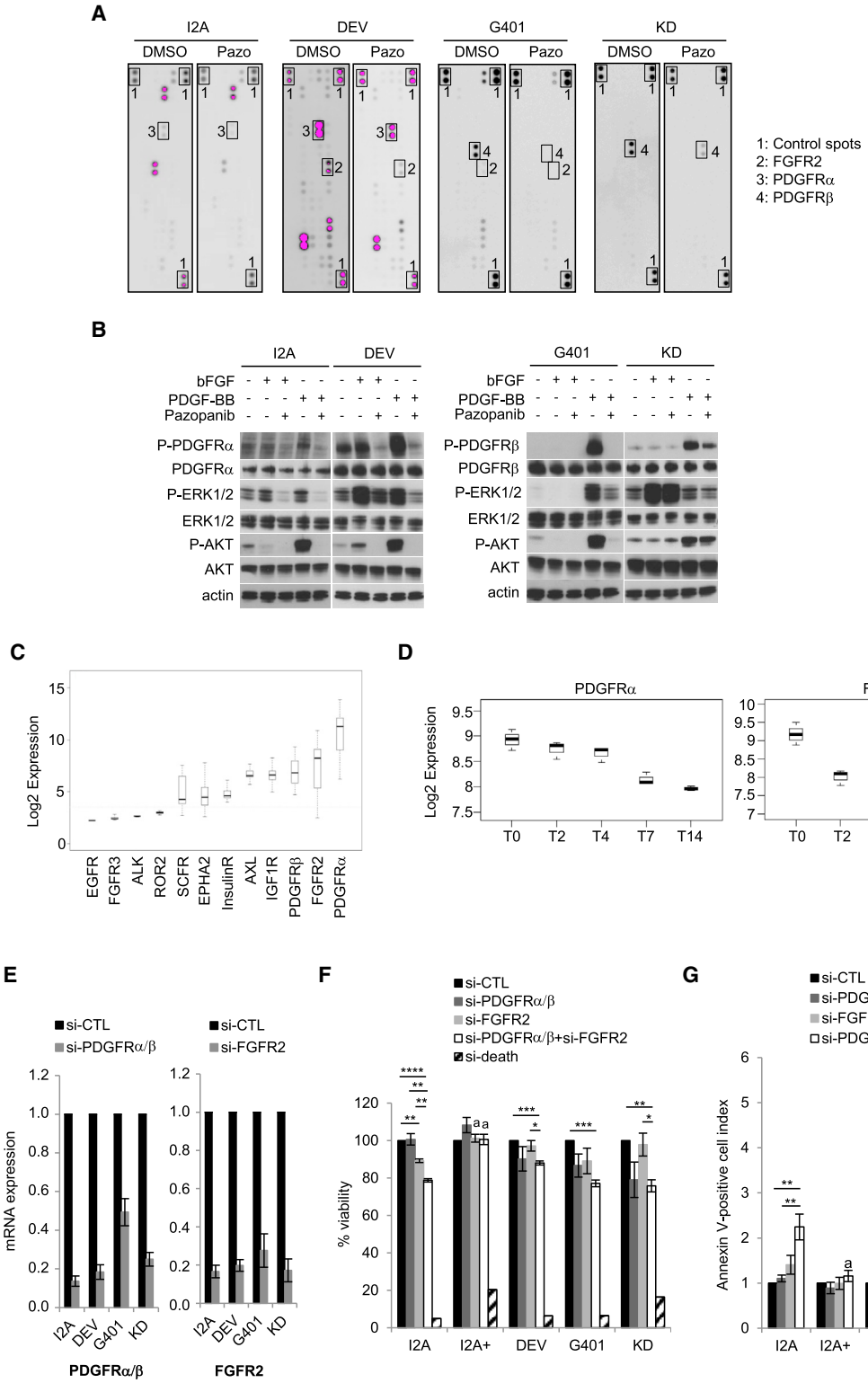

Figure 2. PDGFRα/β and FGFR2 Are Targeted by Pazopanib

(A) Phospho-RTK array showing the inhibitory effects of pazopanib on the phosphorylation of multiple RTKs in I2A, DEV, G401, and KD cell lines. Vertical pairs of spots represent one receptor; control (1), FGFR2 (2), PDGFRα (3), and PDGFRβ (4) are boxed.

(B) Immunoblot of PDGFRα, PDGFRβ, ERK1/2, and AKT phosphorylation levels in I2A, DEV, G401, and KD cell lines after overnight starvation, bFGF or PDGF-BB stimulation, and pazopanib treatment.

(legend continued on next page)

in vivo testing was reported. This result was supported by the Genomics of Drug Sensitivity in Cancer Project, where the cytotoxicity of 130 anticancer drugs on almost 700 cancer cell lines was tested (Garnett et al., 2012); the only 2 drugs showing a cytotoxic effect in the 2 SMARCB1-negative cell lines (G401 and G402) were pazopanib and nutlin-3a. From subsequent *in vitro* resistance-based experiments and primary tumor expression profiling, Wong et al. (2016) identified PDGFRα and FGFR1 as potential oncogenic drivers in RTs and emphasized the necessity of dual RTK depletion to circumvent resistance mechanisms. Finally, Torchia et al. (2016) reported some ability of dasatinib to delay BT12 xenograft growth and showed that PDGFRβ expression, targeted by dasatinib, is epigenetically controlled by SMARCB1 in a subgroup of AT/RT. Altogether, consistent with our own findings, several recent studies converge to identify PDGFRα, PDGFRβ, and FGFRs as potential oncogenic actors in RTs, although their expression profiles may vary according to cell line or primary tumor subtype. How these results will translate into the clinic is a major upcoming issue. The bottleneck of several previously published studies resides in the absence of confirmation in faithful *in vivo* models. In our hands, pazopanib showed actual growth delay on two extra-cranial RT PDXs as a single agent. However, it did not enable sustainable tumor control, which emphasizes the necessity for drug combination. Combining TKi's with other drugs that can act synergistically to lower its IC_{50} will thus be necessary.

The second drug we identified in our screen is CfT, an antiarrhythmic agent. Interestingly, several studies also provide some evidence of unexpected antitumor effects of antiarrhythmic agents. Amiodarone, nimodipine, and verapamil, three major antiarrhythmic agents used in the clinic, showed cytotoxicity on cancer cells (Kubiak et al., 1989; Durmaz et al., 1999). In line with our observation of a metabolic effect of Cft, recent data have shown that targeting a potassium channel can lead to selective apoptosis of cancer cells via reactive oxygen species (Leanza et al., 2017). The potential dependence of RT cell lines on protein metabolism and their sensitivity to endoplasmic reticulum stress provides therapeutic and biological perspectives.

In conclusion, our study provides evidence that exploiting vulnerability to TKi's in SMARCB1-deficient tumors may be an effective therapeutic strategy. Pazopanib has been approved in the treatment of various sarcomas in adults, and a pediatric phase 1 with a liquid formulation has been published (Glade Bender et al., 2013). Whether its use in combination with downstream effector inhibitors or CfT will affect tumor response deserves to be tested in a clinical trial.

EXPERIMENTAL PROCEDURES

Cell Lines

The drug screening was performed on G401 cells (ATCC CRL-1441) and on the inducible system I2A, derived from MON as previously published by our team (Medjkane et al., 2004). Five other human cell lines were used: KD (Versteege et al., 1998), 2004 (Versteege et al., 1998), DEV (Giraudon et al., 1993), Wa2 (Handgretinger et al., 1990), and LM (Versteege et al., 1998). Four cell lines were used as controls: A673 (Ewing sarcoma), DAOY (medulloblastoma), A549 (SMARCA4-deficient lung carcinoma; obtained from the ATCC [CRL-1598, HTB-186, and CCL-185, respectively]), and SK-N-BE(2)C (neuroblastoma) (Barnes et al., 1981). Details for cell culture conditions are described in Supplemental Experimental Procedures.

Compound Screening Workflow

For toxicity screening, cells were plated out in 384-well thin-bottom imaging plates for 24 hr. The Prestwick Chemical Library V2 (Prestwick Chemical), a collection of 1,200 off-patent drugs already approved by the FDA, was then added to a final dose of 10 μM in each well. 48 hr after compound transfer, cells were stained with 0.2 μg/mL DAPI. Images of the DAPI channel (4 fields/well) were acquired using the IN Cell Analyzer 2000 automated wide-field system (GE Healthcare). The drug screening was performed in two independent experiments for each cell line.

Screening Data Analysis

The raw cell count was transformed with log function and normalized using plate median methods and variance adjusted using B-score normalization (Mosteller and Tukey, 1977; Birmingham et al., 2009). RZ score transformations were applied to center and scale the data across the screen. The screening data from each cell-replicate pair was treated individually. RZ scores for a given compound were then mean summarized per replicate screen. Drugs were then ranked based on a maximum RZ score and hits picked on the selection criteria shown in Figure S1B. Details are provided in Supplemental Experiment Procedures.

Cell Viability Assay

For IC_{50} determination, cell viability was assessed using a resazurin assay after 48 hr of drug exposure. IC_{50} data were generated from nonlinear fit of dose-response curves using a four-parameter regression fit in PRISM 5 software (GraphPad). Details are provided in Supplemental Experiment Procedures.

Analysis of Apoptosis

Cells (including supernatant) were harvested 72 hr after treatment or transfection and stained with APC-Annexin V (BD Biosciences) and 7-aminoactinomycin D (Life Technologies). I2A cells were treated or transfected at day 1 after doxycycline withdrawal. Samples were assayed on an LSR II flow cytometer

(C) Ordered boxplots showing log2 expression of RTKs for which phosphorylation was inhibited by pazopanib in more than one cell line, obtained on Affymetrix U133Plus2.0 arrays in 48 human primary RTs (Han et al., 2016). Central rectangles span the first quartile to the third quartile, the horizontal line shows the median, and whiskers are taken to 1.5× interquartile range (IQR) from the quartile.

(D) Log2 expression of *PDGFRα* and *FGFR2* obtained on Affymetrix HuGene 2.1st arrays in I2A at different time points (days) after doxycycline withdrawal. Central rectangles span the first quartile to the third quartile; the horizontal line shows the median; whiskers are taken to 1.5 × IQR from the quartile.

(E) qRT-PCR analysis of knockdown efficacy of siRNAs used to silence PDGFRα or FGFR2 (I2A and DEV) and PDGFRβ or FGFR2 (G401 and KD). Data were normalized to siRNA control (si-CTL) and are shown as the mean ± SEM of results obtained with 3 different siRNAs against PDGFRα, 2 different siRNAs against PDGFRβ, and 2 different siRNAs against FGFR2.

(F and G) Cell viability (F) and Annexin V staining (G) upon siRNA silencing of PDGFRα, FGFR2, and the combination in I2A, I2A+, and DEV cells and of PDGFRβ, FGFR2, and the combination in G401 and KD cells. Death-siRNA was used as a positive control of cell mortality. Data were normalized to si-CTL and are shown as the mean ± SEM of results obtained with 3 different siRNAs against PDGFRα, 2 different siRNAs against PDGFRβ, and 2 different siRNAs against FGFR2 (n = 3–4 independent experiments). For each gene, the siRNA inducing the higher depletion of its target considering the qRT-PCR results was used in dual depletion experiments. ns, not significant; *p < 0.05; **p < 0.01; ***p < 0.001; ****p < 0.0001; a, p < 0.05 versus I2A of the same transfection (two-tailed unpaired Student's t test).

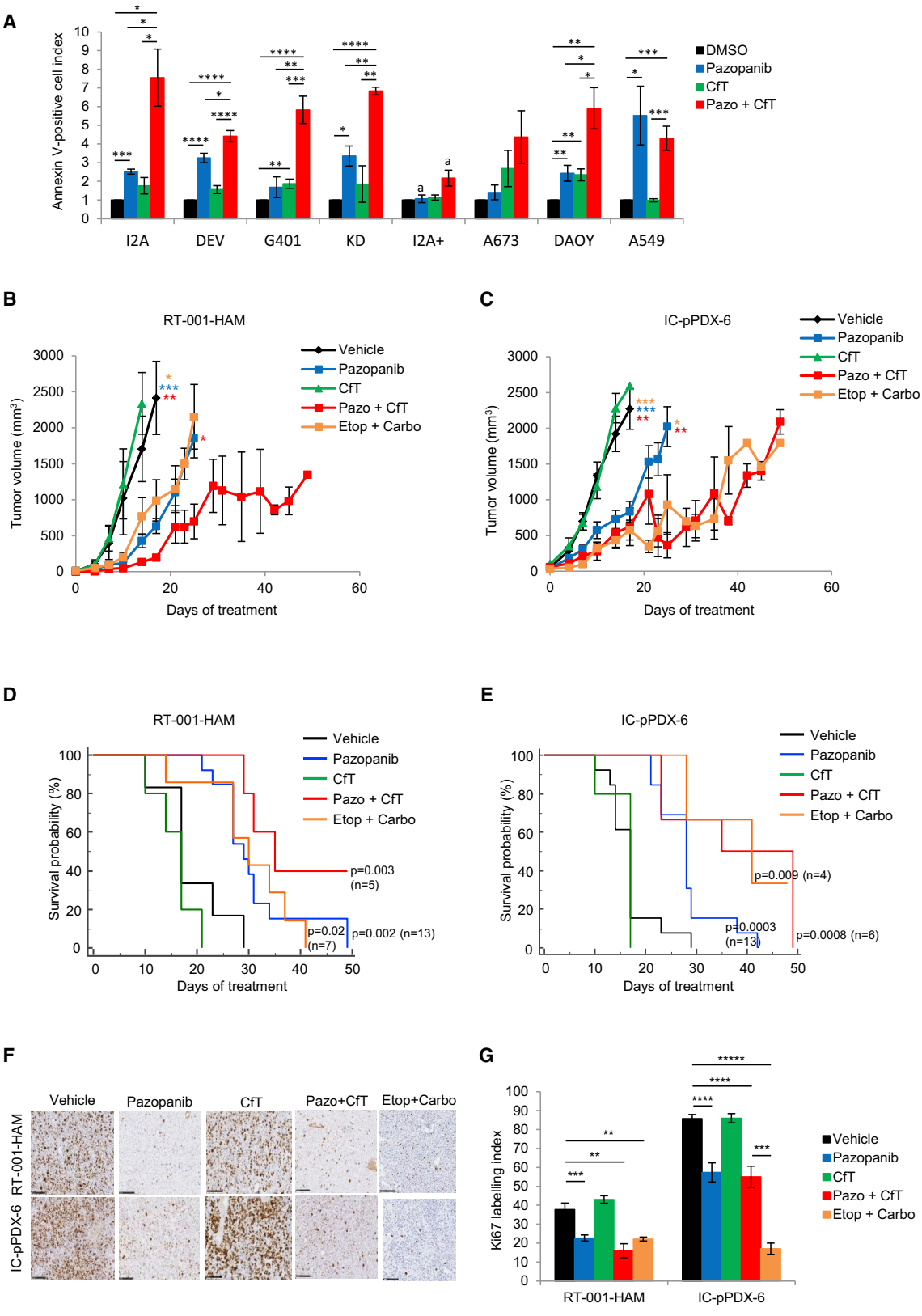

(legend on next page)

(Becton Dickinson). Data were analyzed with FlowJo software (Tree Star), and the Annexin-V-positive cell index was calculated by normalizing the percentage of Annexin-V-positive cells to control.

Human Phospho-Receptor Tyrosine Kinase Array

The human phospho-RTK Array kit for 49 RTKs (R&D Systems) was used to simultaneously detect the relative tyrosine phosphorylation levels. A total of 4×10^6 I2A cells with doxycycline, G401, DEV, and KD cells were seeded in 25-cm^2 flasks 1 day before treatment with pazopanib at IC_{50} concentrations or DMSO as a control. Cells were then harvested after 30 min of treatment, and the RTK array analysis was performed as described in Supplemental Experimental Procedures. For phospho-array validation experiments, cells underwent overnight serum starvation and were stimulated with 25 ng/mL of bFGF (Sigma-Aldrich) or 50 ng/mL of PDGF-BB (Millipore) in the presence or absence of pazopanib at IC_{50} concentrations. Details regarding cell extraction and western blotting are given in Supplemental Experiment Procedures.

Transient Transfections

The procedures for transfections are detailed in Supplemental Experimental Procedures.

RNA Extraction, Reverse Transcription, and qRT-PCR

Details are provided in Supplemental Experimental Procedures.

RNA-Seq Analyses

RNA from DEV and G401 cells were extracted 48 hr after initiation of treatment with CfT from 3 independent experiments. mRNA expression was assessed using the Illumina HiSeq2500 platform. Data processing and analyses are detailed in Supplemental Experimental Procedures.

Patient-Derived Xenograft Studies

Two RT PDX models were used: RT-001-HAM (liver tumor; Nicolle et al., 2016) and IC-pPDX-6 (soft tissue; Curie Institute). Drug effects were assessed in Swiss nude mice. Treatment modalities and assessment of efficacy are detailed in the Supplemental Experimental Procedures. The project was approved per the Curie Institute ethical committee (approval no. 05191.4); all experiments were performed in compliance with ethical requirements.

Statistical Methods

Experimental results are representative of at least two independent experiments. *In vivo* experiments were performed with at least four mice per group. The statistical significance of data in all figures was evaluated by Student's t test.

DATA AND SOFTWARE AVAILABILITY

The accession numbers for the I2A microarray gene expression data and the CfT-treated G401 and DEV RNA-seq data are GEO: GSE98277 and GEO: GSE102467, respectively.

SUPPLEMENTAL INFORMATION

Supplemental Information includes Supplemental Experimental Procedures, four figures, one table, and one data set and can be found with this article online at https://doi.org/10.1016/j.celrep.2017.10.076.

AUTHOR CONTRIBUTIONS

Conceptualization, F.B and C.C.; Methodology, C.C., E.D.N., and F.B.; Investigation, C.C., A. Leruste, Z.-Y.H., A.T.-E., M.B., and E.A.; Validation, C.C.; Formal Analysis and Visualization, M.A., A. Lescure, and W.R.; Resources, D.S., S.Z., S.C., M.-M.A., L.M., S.B., and J.M.-P.; Writing – Original Draft, C.C. and F.B.; Writing – Review & Editing, C.C., F.B., and O.D.; Supervision, F.B. and O.D.; Funding Acquisition, F.B., S.R.-R., and O.D.

ACKNOWLEDGMENTS

We thank the Experimental Pathology Platform (PATHEX) of the Curie Institute for its support of the immunohistochemistry experiments. We thank the Laboratoire d'Investigations Précliniques, Franck Assayag, and Elisabetta Marangoni for their expert advice and technical support. We thank Sophie Brancherreau for her involvement in establishing PDX and Joshua Waterfall for helpful discussions. The RTOP team is supported by the SiRIC-Curie Program (grant INCa-DGOS-4654). INSERM U830 is supported by the Institut National de la Santé et de la Recherche Médicale, the Curie Institute, and the Ligue Nationale Contre Le Cancer. This study was supported by a grant from the French Ministry of Health (Direction Générale de l'Organisation des Soins) and the French National Cancer Institute (PRTKRTK-2012, grant 2012-1-RT-02-IC-1). We thank the associations that support our research on Rhabdoid Tumors: Abigael, Marabout de Ficelle, Franck un Rayon de Soleil, Les Torocinelles, Couleur Jade, Au nom d'Andrea, and ADAM. We are also indebted to the SFCE, the Enfants et Santé Federation, and Etoile de Martin for their financial support. F.B. is a recipient of the fellowship Enfance-et-Cancer/Hubert Gouin Association. The Biophenics High-Content Screening Laboratory received support under the program Paris Alliance of Cancer Research Institutes, PACRI, "Investissements d'Avenir" launched by the French Government and implemented by the ANR with the reference ANR-11-PHUC-002. Expression profiling was performed by the Département de Transfert & Plateforme Génomique of the Curie Institute. High-throughput sequencing was performed by the ICGex NGS platform of the Curie Institute, which is supported by grants ANR-10-EQPX-03 (Equipex) and ANR-10-INBS-09-08 (France Génomique Consortium) from the Agence Nationale de la Recherche ("Investissements d'Avenir" program), by the Canceropole Ile-de-France, and by the SiRIC-Curie Program (grant INCa-DGOS-4654).

Received: March 24, 2017
Revised: August 8, 2017
Accepted: October 19, 2017
Published: November 14, 2017

REFERENCES

Barnes, E.N., Biedler, J.L., Spengler, B.A., and Lyser, K.M. (1981). The fine structure of continuous human neuroblastoma lines SK-N-SH, SK-N-BE(2), and SK-N-MC. In Vitro *17*, 619–631.

Bertolini, F., Sukhatme, V.P., and Bouche, G. (2015). Drug repurposing in oncology: patient and health systems opportunities. Nat. Rev. Clin. Oncol. *12*, 732–742.

Birmingham, A., Selfors, L.M., Forster, T., Wrobel, D., Kennedy, C.J., Shanks, E., Santoyo-Lopez, J., Dunican, D.J., Long, A., Kelleher, D., et al. (2009).

Figure 3. *In Vitro* and *In Vivo* Treatment with Pazopanib and CfT

(A) Annexin V staining in the indicated cell lines after treatment with pazopanib, CfT, or the combination, normalized to DMSO control. Data are shown as the mean ± SEM (n = 3–8 independent experiments). ns, not significant; *p < 0.05; **p < 0.01; ***p < 0.001; ****p < 0.00001; a, p < 0.05 versus I2A of the same treatment (two-tailed unpaired Student's t test).

(B–E) Tumor volume (B and C) and Kaplan-Meier survival curves (D and E) of RT-001-HAM (B and D) and IC-pPDX-6 (C and E) RT PDXs treated with pazopanib, CfT, both combined, or the etoposide-carboplatin combination. ns, not significant; *p < 0.05; **p < 0.01; ***p < 0.001 (two-tailed unpaired Student's t test). Data in (B) and (C) are shown as the mean of tumor volume ± SEM (n = 4–13 mice for each group). p values in (D) and (E) compared drug-treated groups with the vehicle-treated group.

(F and G) Ki67 immunostaining images (F) and data (G) are shown as the mean of Ki67 labeling index ± SEM. Scale bar represents 100 μm. ns, not significant; *p < 0.05; **p < 0.01; ***p < 0.001; ****p < 0.0001; *****p < 0.00001 (two-tailed unpaired Student's t test).

Statistical methods for analysis of high-throughput RNA interference screens. Nat. Methods *6*, 569–575.

Brennan, B., De Salvo, G.L., Orbach, D., De Paoli, A., Kelsey, A., Mudry, P., Francotte, N., Van Noesel, M., Bisogno, G., Casanova, M., and Ferrari, A. (2016). Outcome of extracranial malignant rhabdoid tumours in children registered in the European Paediatric Soft Tissue Sarcoma Study Group Non-Rhabdomyosarcoma Soft Tissue Sarcoma 2005 Study-EpSSG NRSTS 2005. Eur. J. Cancer *60*, 69–82.

D'cunja, J., Shalaby, T., Rivera, P., von Büren, A., Patti, R., Heppner, F.L., Arcaro, A., Rorke-Adams, L.B., Phillips, P.C., and Grotzer, M.A. (2007). Antisense treatment of IGF-IR induces apoptosis and enhances chemosensitivity in central nervous system atypical teratoid/rhabdoid tumours cells. Eur. J. Cancer *43*, 1581–1589.

Durmaz, R., Deliorman, S., Uyar, R., Işiksoy, S., Erol, K., and Tel, E. (1999). The effects of anticancer drugs in combination with nimodipine and verapamil on cultured cells of glioblastoma multiforme. Clin. Neurol. Neurosurg. *101*, 238–244.

Garnett, M.J., Edelman, E.J., Heidorn, S.J., Greenman, C.D., Dastur, A., Lau, K.W., Greninger, P., Thompson, I.R., Luo, X., Soares, J., et al. (2012). Systematic identification of genomic markers of drug sensitivity in cancer cells. Nature *483*, 570–575.

Geoerger, B., Bourdeaut, F., DuBois, S.G., Fischer, M., Geller, J.I., Gottardo, N.G., Marabelle, A., Pearson, A.D.J., Modak, S., Cash, T., et al. (2017). A phase I study of the CDK4/6 inhibitor Ribociclib (LEE011) in pediatric patients with malignant rhabdoid tumors, neuroblastoma, and other solid tumors. Clin. Cancer Res. *23*, 2433–2441.

Giraudon, P., Dufay, N., Hardin, H., Reboul, A., Tardy, M., and Belin, M.F. (1993). Differentiation of a medulloblastoma cell line towards an astrocytic lineage using the human T lymphotropic retrovirus-1. Neuroscience *52*, 1069–1079.

Glade Bender, J.L., Lee, A., Reid, J.M., Baruchel, S., Roberts, T., Voss, S.D., Wu, B., Ahern, C.H., Ingle, A.M., Harris, P., et al. (2013). Phase I pharmacokinetic and pharmacodynamic study of pazopanib in children with soft tissue sarcoma and other refractory solid tumors: a children's oncology group phase I consortium report. J. Clin. Oncol. *31*, 3034–3043.

Han, Z.-Y., Richer, W., Fréneaux, P., Chauvin, C., Lucchesi, C., Guillemot, D., Grison, C., Lequin, D., Pierron, G., Masliah-Planchon, J., et al. (2016). The occurrence of intracranial rhabdoid tumours in mice depends on temporal control of Smarcb1 inactivation. Nat. Commun. *7*, 10421.

Handgretinger, R., Kimmig, A., Koscielnak, E., Schmidt, D., Rudolph, G., Wolburg, H., Paulus, W., Schilbach-Stueckle, K., Ottenlinger, C., Menrad, A., et al. (1990). Establishment and characterization of a cell line (Wa-2) derived from an extrarenal rhabdoid tumor. Cancer Res. *50*, 2177–2182.

Huang, P.H. (2017). Targeting SWI/SNF mutant cancers with tyrosine kinase inhibitor therapy. Expert Rev. Anticancer Ther. *17*, 1–3.

Johann, P.D., Erkek, S., Zapatka, M., Kerl, K., Buchhalter, I., Hovestadt, V., Jones, D.T.W., Sturm, D., Hermann, C., Segura Wang, M., et al. (2016). Atypical teratoid/rhabdoid tumors are comprised of three epigenetic subgroups with distinct enhancer landscapes. Cancer Cell *29*, 379–393.

Kerl, K., Ries, D., Unland, R., Borchert, C., Moreno, N., Hasselblatt, M., Jürgens, H., Kool, M., Görlich, D., Eveslage, M., et al. (2013). The histone deacetylase inhibitor SAHA acts in synergism with fenretinide and doxorubicin to control growth of rhabdoid tumor cells. BMC Cancer *13*, 286.

Knutson, S.K., Warholic, N.M., Wigle, T.J., Klaus, C.R., Allain, C.J., Raimondi, A., Porter Scott, M., Chesworth, R., Moyer, M.P., Copeland, R.A., et al. (2013). Durable tumor regression in genetically altered malignant rhabdoid tumors by inhibition of methyltransferase EZH2. Proc. Natl. Acad. Sci. USA *110*, 7922–7927.

Kubiak, C., Couvreur, P., Manil, L., and Clausse, B. (1989). Increased cytotoxicity of nanoparticle-carried Adriamycin in vitro and potentiation by verapamil and amiodarone. Biomaterials *10*, 553–556.

Leanza, L., Romio, M., Becker, K.A., Azzolini, M., Trentin, L., Managò, A., Venturini, E., Zaccagnino, A., Mattarei, A., Carraretto, L., et al. (2017). Direct pharmacological targeting of a mitochondrial ion channel selectively kills tumor cells in vivo. Cancer Cell *31*, 516–531.e10.

Medjkane, S., Novikov, E., Versteege, I., and Delattre, O. (2004). The tumor suppressor hSNF5/INI1 modulates cell growth and actin cytoskeleton organization. Cancer Res. *64*, 3406–3413.

Mosteller, F., and Tukey, J.W. (1977). Data Analysis and Regression: A Second Course in Statistics (Pearson).

Muscat, A., Popovski, D., Jayasekara, W.S.N., Rossello, F.J., Ferguson, M., Marini, K.D., Alamgeer, M., Algar, E.M., Downie, P., Watkins, D.N., et al. (2016). Low-dose histone deacetylase inhibitor treatment leads to tumor growth arrest and multi-lineage differentiation of malignant rhabdoid tumors. Clin. Cancer Res. *22*, 3560–3570.

Nicolle, D., Fabre, M., Simon-Coma, M., Gorse, A., Kappler, R., Nonell, L., Mallo, M., Haidar, H., Déas, O., Mussini, C., et al. (2016). Patient-derived mouse xenografts from pediatric liver cancer predict tumor recurrence and advise clinical management. Hepatology *64*, 1121–1135.

Raynal, N.J.-M., Da Costa, E.M., Lee, J.T., Gharibyan, V., Ahmed, S., Zhang, H., Sato, T., Malouf, G.G., and Issa, J.J. (2017). Repositioning FDA-approved drugs in combination with epigenetic drugs to reprogram colon cancer epigenome. Mol. Cancer Ther. *16*, 397–407.

Robison, N.J., Campigotto, F., Chi, S.N., Manley, P.E., Turner, C.D., Zimmerman, M.A., Chordas, C.A., Werger, A.M., Allen, J.C., Goldman, S., et al. (2014). A phase II trial of a multi-agent oral antiangiogenic (metronomic) regimen in children with recurrent or progressive cancer. Pediatr. Blood Cancer *61*, 636–642.

Singh, A., Lun, X., Jayanthan, A., Obaid, H., Ruan, Y., Strother, D., Chi, S.N., Smith, A., Forsyth, P., and Narendran, A. (2013). Profiling pathway-specific novel therapeutics in preclinical assessment for central nervous system atypical teratoid rhabdoid tumors (CNS ATRT): favorable activity of targeting EGFR- ErbB2 signaling with lapatinib. Mol. Oncol. *7*, 497–512.

Smith, M.E., Cimica, V., Chinni, S., Challagulla, K., Mani, S., and Kalpana, G.V. (2008). Rhabdoid tumor growth is inhibited by flavopiridol. Clin. Cancer Res. *14*, 523–532.

Torchia, J., Golbourn, B., Feng, S., Ho, K.C., Sin-Chan, P., Vasiljevic, A., Norman, J.D., Guilhamon, P., Garzia, L., Agamez, N.R., et al. (2016). Integrated (epi)-genomic analyses identify subgroup-specific therapeutic targets in CNS rhabdoid tumors. Cancer Cell *30*, 891–908.

Versteege, I., Sévenet, N., Lange, J., Rousseau-Merck, M.F., Ambros, P., Handgretinger, R., Aurias, A., and Delattre, O. (1998). Truncating mutations of hSNF5/INI1 in aggressive paediatric cancer. Nature *394*, 203–206.

Wang, X., Lee, R.S., Alver, B.H., Haswell, J.R., Wang, S., Mieczkowski, J., Drier, Y., Gillespie, S.M., Archer, T.C., Wu, J.N., et al. (2017). SMARCB1-mediated SWI/SNF complex function is essential for enhancer regulation. Nat. Genet. *49*, 289–295.

Wöhrle, S., Weiss, A., Ito, M., Kauffmann, A., Murakami, M., Jagani, Z., Thuery, A., Bauer-Probst, B., Reimann, F., Stamm, C., et al. (2013). Fibroblast growth factor receptors as novel therapeutic targets in SNF5-deleted malignant rhabdoid tumors. PLoS ONE *8*, e77652.

Wong, J.P., Todd, J.R., Finetti, M.A., McCarthy, F., Broncel, M., Vyse, S., Luczynski, M.T., Crosier, S., Ryall, K.A., Holmes, K., et al. (2016). Dual targeting of PDGFRα and FGFR1 displays synergistic efficacy in malignant rhabdoid tumors. Cell Rep. *17*, 1265–1275.